Modifying Mie Resonances and Carrier Dynamics of Silicon Nanoparticles by Dense Electron-Hole Plasmas

Jin Xiang,[1] Jingdong Chen,[2] Qiaofeng Dai,[1] Shaolong Tie,[3] Sheng Lan,[1,*] and
Andrey E. Miroshnichenko[4,†]

[1]*Guangdong Provincial Key Laboratory of Nanophotonic Functional Materials and Devices, School of Information and Optoelectronic Science and Engineering, South China Normal University, Guangzhou 510006, China*

[2]*College of Physics and Information Engineering, Minnan Normal University, Zhangzhou 363000, China*

[3]*School of Chemistry and Environment, South China Normal University, Guangzhou 510006, China*

[4]*School of Engineering and Information Technology, University of New South Wales, Canberra, ACT 2600, Australia*

The strongly localized electric field achieved at the Mie resonances of a silicon nanoparticle enables the generation of a large carrier density, which offers us the opportunity to manipulate the linear and nonlinear optical properties of silicon nanoparticles by optically injecting a dense electron-hole plasma. Here, we show that the dense electron-hole plasma created in a silicon nanoparticle significantly modifies the complex dielectric constant of silicon, which in turn leads to wavelength shift and amplitude change in the magnetic dipole resonance. We demonstrate that the maximum wavelength shift of the magnetic dipole resonance can be revealed by exploiting the hot-electron luminescence emitted by the silicon nanoparticle, which acts as a built-in light source with a broad bandwidth and a short lifetime. We demonstrate that the quantum efficiency of the hot-electron luminescence of silicon nanoparticles can be enhanced a factor of more than 5 through the injection of a dense electron-hole plasma. More interestingly, an acceleration of the radiative recombination process is found at high carrier densities. Our findings are helpful for understanding the modification of Mie resonances in silicon nanoparticles induced by the dense electron-hole plasmas and useful for designing silicon-based photonic devices.

I. INTRODUCTION

As one of the most important semiconductors, Si has been used to fabricate electronic devices, waveguides, detectors, solar cells, etc. [1] Owing to its indirect band gap, however, the achievement of efficient Si-based emitters remains a big challenge. Although quantum dots from Si that are smaller than 10 nm have been demonstrated [2], they are difficult to integrate into Si-based waveguides. Therefore, efficient Si-based photon emitters with a feature size of approximately 200 nm, which can be fabricated using the current fabrication technology of Si chips and integrated with other devices into photonic circuits, are highly desirable.

Metamaterials and metasurfaces capable of realizing various functions have been actively studied in the past two decades [3–5]. In the microwave and terahertz spectral ranges, metal wires and split-ring resonators function as artificial electric and magnetic meta-atoms supporting electric dipoles (EDs) and magnetic dipoles (MDs), respectively [6,7]. Unfortunately, metamaterials or metasurfaces composed of such meta-atoms fail to work at optical frequencies owing to the large ohmic loss of metals.

As an alternative to the building blocks for metamaterials or metasurfaces operating at optical frequencies, dielectric nanoparticles with large refractive indices have attracted a great deal of interest, because they support both the ED and MD resonances and act simultaneously as artificial electric and magnetic meta-atoms [8–12]. Typical examples include silicon (Si), germanium, and gallium arsenide nanoparticles, which exhibit distinct MD and/or ED and even magnetic quadrupole (MQ) and electric quadrupole (EQ) resonances in their scattering spectra. These Mie resonances can be employed to enhance the nonlinear optical responses of nanoparticles [13,14] and to manipulate light scattering from nanoantennas and light emission from nanomaterials [15,16].

Since the ED and MD resonances of a nanoparticle depend strongly on the complex refractive index of the

---

*slan@scnu.edu.cn
†andrey.miroshnichenko@unsw.edu.au

material, static and dynamical modulation in the optical properties of single nanoparticles or metadevices can be realized by injecting electron-hole plasmas into the nanoparticles [17–21]. Very recently, it has been demonstrated that the ED and MD resonances of Si nanoparticles can be employed to significantly enhance two- and three-photon-induced absorption (2PA and 3PA, respectively), while the EQ and MQ resonances can be utilized to enhance the emission of hot-electron luminescence [14]. Since the 2PA and 3PA of a Si nanoparticle can be enhanced by factors of approximately 55 and approximately 500, carrier densities larger than 10^{20} cm^{-3} can be readily generated in the Si nanoparticle, leading to the emission of broadband hot-electron luminescence [14].

In principle, it is anticipated that the strongest luminescence can be achieved by resonantly exciting the MD resonance. However, a blue shift of the MD resonance is expected if the refractive-index change of Si induced by the injected plasma is taken into account [19,21]. Apart from injected carriers, the complex refractive index of Si is also affected by the temperature rise in Si nanoparticles, which introduces a red shift of the MD resonance [22]. An understanding of the optical response and carrier dynamics of a single Si nanoparticle in the presence of dense electron-hole plasmas is quite important for practical applications of Si nanoparticles in active photonic devices, such as optical switches, broadband light sources, and even nanolasers. On the other hand, the blue shift of the MD resonance provides a simple and effective way of characterizing the carrier density generated in the Si

nanoparticle, from which the quantum efficiency can easily be deduced.

Basically, the blue shift of the MD resonance of a Si nanoparticle excited by femtosecond laser pulses is dynamical and it follows the generation and decay of the electron-hole plasma. A pump-probe experiment, in which the probe pulse is a supercontinuum with an appropriate delay with respect to the pump pulse, is necessary to record the evolution of the scattering spectrum, as schematically illustrated in Fig. 1. Although such a technique has been successfully employed to characterize the carrier dynamics in bulk materials and metasurfaces [18,23], its application in measuring the transient scattering spectra of a single nanoparticle remains a big challenge for two reasons. First, the extremely small scattering cross section (approximately 10^{14} m^{-2}) of the nanoparticle requires a white light source with a large power (e.g., a 150-W lamp) in order to achieve a detectable scattering intensity with reasonable signal-to-noise ratio. Unfortunately, the average power of the supercontinuum generated by pumping a nonlinear photonic fiber does not satisfy this requirement. Second, the measurement system must be stable enough to avoid any shift of the laser focus point from the nanoparticle during the measurement, because the nonlinear optical processes involved are extremely sensitive to the slight change of the excitation intensity.

In this paper, we realize modification of the Mie resonances and carrier dynamics of silicon nanoparticles by injecting dense electron-hole plasmas. It can be characterized by measuring either the excitation spectrum of the
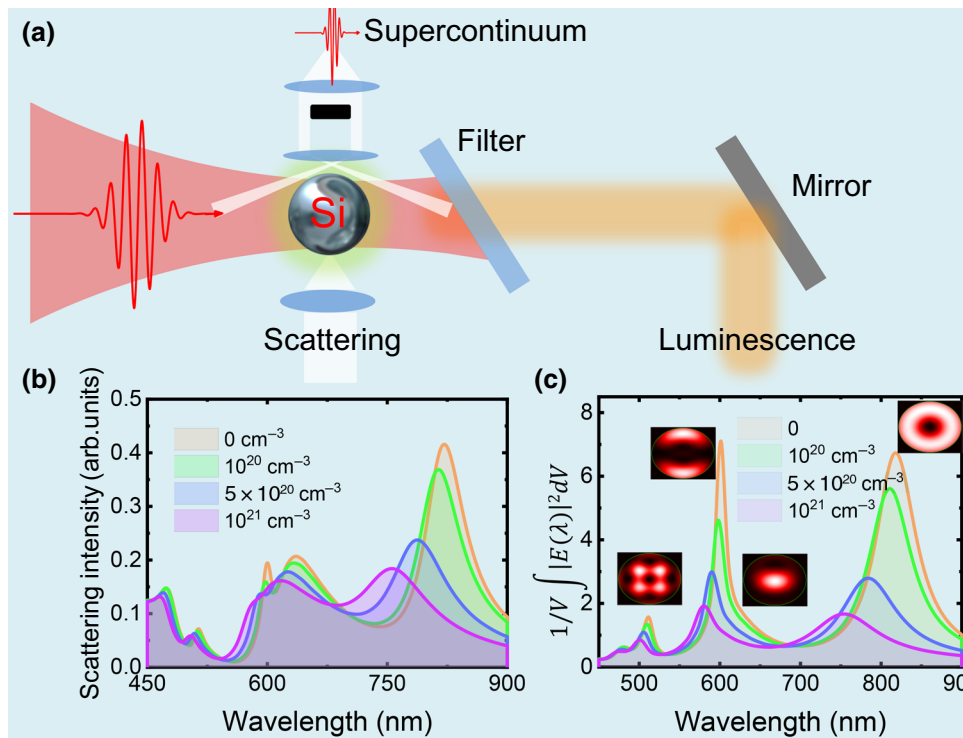

FIG. 1. Virtualizing MD resonance shift by using hot-electron luminescence. (a) A schematic showing the principle of using the broadband hot-electron luminescence emitted by a Si nanoparticle to virtualize the MD-resonance shift of the Si nanoparticle induced by dense electron-hole plasmas. (b) The evolution of the scattering spectrum of a Si nanosphere with $d \sim 200$ nm with increasing density of the electron-hole plasma. (c) The evolution of the electrical energy $\left[\int |E(\lambda)|^2 dV\right]/V$ spectrum calculated for the Si nanosphere with increasing density of the electron-hole plasma. The electric field distributions calculated at the MD, ED, MQ, and ED resonances are shown as insets.

luminescence or the MD-enhanced luminescence. The carrier density generated in the Si nanoparticle and thus the quantum efficiency of the luminescence can be extracted from the blue shift of the MD resonance. A significant enhancement in the radiative recombination rate is observed at high densities of electron-hole plasmas.

II. METHODS

A. Sample preparation

Si nanoparticles with diameters ranging from 50 to 300 nm are fabricated using femtosecond laser ablation of a Si wafer immersed in water. A femtosecond laser amplifier (Legend, Coherent) with a pulse duration of 100 fs and a repetition rate of 1 kHz is employed in the ablation process. An objective with a focal length of 25 cm is used to focus the femtosecond laser beam on the Si wafer with a spot diameter of approximately 40 μm. Si nanoparticles ejected from the Si wafer after the irradiation of femtosecond laser light are uniformly dispersed in water. Once the ablation is completed, the aqueous solution containing Si nanoparticles is centrifuged at 5000 rpm to separate Si nanoparticles with diameters of 50–300 nm from other particles. The Si nanoparticles are dispersed on an ITO substrate for morphology characterization and on a glass slide for optical characterization. The composition and crystalline phase of the fabricated Si nanoparticles are examined using high-resolution scanning electron microscopy and transmission-electron microscopy. Each Si nanoparticle is composed of a single crystalline core and a very thin amorphous shell on the surface (see the Supplemental Material, S1 [24]).

B. Experimental setup

The scattering spectra of the Si nanoparticles are measured using a dark-field microscope (Observer A1, Zeiss). The characterization of the nonlinear optical properties of the Si nanoparticles is carried out using a femtosecond laser oscillator (Mira-HP, Coherent) and an optical parametric oscillator (Mira OPO-X, Coherent) with a pulse duration of 130 fs and a repetition rate of 76 MHz. The femtosecond laser light is introduced into an inverted microscope and focused on Si nanoparticles using a 100× objective. The nonlinear optical signals from the Si nanoparticles are collected by the same objective and directed to a spectrometer (SR500, Andor) for analysis.

C. Numerical modeling

The scattering spectra of the Si nanoparticles placed on a glass slide is calculated using Mie theory or simulated using the finite-difference time-domain (FDTD) technique, using LUMERICAL [25]. In the FDTD simulation, a nonuniform mesh size with the smallest mesh size of 1 nm as well as a perfectly matched boundary condition is employed.

III. RESULTS AND DISCUSSION

The Si nanoparticles used in this work are fabricated using femtosecond laser ablation [14,26]. The linear and nonlinear optical properties of the Si nanoparticles are characterized using dark-field microscopy and a microphotoluminescence measurement system composed of a femtosecond laser, an inverted microscope, a spectrometer, and a charge-coupled device (for details, see Sec. II).

The principle of using the hot-electron luminescence emitted by a Si nanoparticle to characterize the MD resonance shift is depicted in Fig. 1(a). Basically, the MD resonance is determined mainly by the real part of the complex refractive index because the change in the imaginary part is almost negligible (see the Supplemental Material, S2 [24]). It should be emphasized that the hot-electron luminescence emitted by the Si nanoparticles satisfies the three conditions necessary for virtualizing the MD resonance shift [14]. First, it acts as a broadband white-light source. Second, its decay follows exactly the decay of the carrier density with a short lifetime (approximately 50 ps). Finally, its intensity is enhanced at the MD resonance. Previously, enhanced photoluminescence (PL) has generally been observed at the surface-plasmon resonances of plasmonic nanoparticles or nanostructures with negligible shift [27–29], because the carrier density in metallic nanoparticles and nanostructures is quite large (approximately 10^{23} cm^{-3}) as compared with the injected carrier density (approximately 10^{20}–10^{21} cm^{-3}). However, the situation is completely different for semiconductors the complex refractive indices of which can be dramatically modified by dense electron-hole plasmas.

Basically, the dielectric constant of Si (ε), which exhibits a strong dependence on the density of the electron-hole plasma (ρ_{eh}), can be described as follows [21,23]:

$$\varepsilon(\omega) = \varepsilon_{\mathrm{ib}}(\omega^*) \left(1 - \frac{\rho_{\mathrm{eh}}}{\rho_{\mathrm{bf}}}\right) - \frac{\omega_{\mathrm{pl}}^2(\rho_{\mathrm{eh}})}{\omega^2 + 1/\tau_e^2})(1 - i/\omega\tau_e). \tag{1}$$

Here, $\omega^* = \omega + \zeta \rho_{\mathrm{eh}}/\rho_{\mathrm{bgr}}$ is an effective photon frequency that accounts for the ρ_{eh}-dependent band-gap shrinkage effect on interband transitions $\varepsilon_{\mathrm{ib}}(\omega^*)$, $\rho_{\mathrm{bgr}} \approx 1 \times 10^{22}$ cm^{-3} is the characteristic renormalization electron-hole plasma density, $\hbar\zeta \sim 1.7$ eV, and ρ_{bf} is the characteristic band capacity of the specific photoexcited regions of the first Brillouin zone (approximately 4×10^{21} cm^{-3} and approximately 4.5×10^{22} cm^{-3} for L and X valleys in Si). The bulk electron-hole plasma frequency is defined as

$$\omega_{\mathrm{pl}}^2(\rho_{\mathrm{eh}}) = 4\pi \frac{\rho_{\mathrm{eh}} e^2}{\varepsilon_{\mathrm{hf}}(\rho_{\mathrm{eh}}) m_{\mathrm{opt}}^*(\rho_{\mathrm{eh}})}, \tag{2}$$

where $m_{\mathrm{opt}}^* = 0.18 m_e$ is the effective optical mass of the electron-hole pair and $\varepsilon_{\mathrm{hf}}(\rho_{\mathrm{eh}}) = 1 + \varepsilon_{\mathrm{hf}}(0) e^{-\rho_{\mathrm{eh}}/\rho_{\mathrm{scr}}}$

is the high-frequency dielectric constant with $\rho_{scr} \approx 1 \times 10^{21}$ cm^{-3}.

In Eq. (1), we consider the effects of band filling, bandgap renormalization, and free carriers on the complex dielectric constant of Si. At high plasma densities, the effect of free carriers, which can be described by the Drude model, plays a dominant role.

Based on the complex dielectric constant described by Eq. (1), we can calculate the scattering spectra of a Si nanoparticle (e.g., a Si nanosphere with $d = 200$ nm) modified by electron-hole plasma of different densities, as shown in Fig. 1(b). It is noted that the MD resonance of the Si nanosphere is blue shifted, broadened, and attenuated with increasing carrier density, implying the gradual phase transition from semiconductor to metal induced by the dense electron-hole plasma.

Physically, the 2PA and 3PA of a Si nanoparticle can be described by $\int |E(\lambda)|^4 dV/V$ and $\int |E(\lambda)|^6 dV/V$ [14]. Apart from the enhancement in 2PA and 3PA, the MD resonance of the Si nanoparticle can also be utilized to enhance the hot-electron luminescence, with the enhancement factor described by $\int |E(\lambda)|^2 dV/V$. In this case, a large blue shift is expected because of its large internal mode volume, which characterizes the sensitivities of the Mie resonances to the change of the dielectric constant [30] (see the Supplemental Material, S3 [24]). In Fig. 1(c), we present the evolution of the enhancement-factor spectrum with increasing carrier density, which appears to be quite similar to that of the scattering spectrum [see Fig. 1(b)]. Specifically, the spectral shifts are almost the same in the two cases, thus enabling us to characterize the blue shift of the MD resonance by exploiting the MD-enhanced luminescence.

Actually, the scattering cross section of the MD can be expressed as [31]

$$\sigma_{MD} = \frac{k_0^4 \varepsilon_d \mu_0}{6\pi \varepsilon_0 |\mathbf{E}_{inc}|^2} |\mathbf{m}|^2, \qquad (3)$$

where $\mathbf{m} = -(i\omega/2) \int [\mathbf{r}' \times \mathbf{P}(\mathbf{r}')] d\mathbf{r}$ is the magnetic dipole moment and $\mathbf{P}(\mathbf{r}) = \varepsilon_0(\varepsilon_p - \varepsilon_d)\mathbf{E}(\mathbf{r})$ is the polarization. Therefore, one can easily obtain

$$\sigma_{MD} \propto \int |\mathbf{E}/\mathbf{E}_0|^2 dV. \qquad (4)$$

This confirms that the scattering cross section of the MD is also governed by $\int |E(\lambda)|^2 dV/V$.

In Fig. 1(c), we show the evolution of the spectrum of $\int |E(\lambda)|^2 dV/V$ with increasing carrier density. A similar blue shift is also observed in the spectra of $\int |E(\lambda)|^4 dV/V$ and $\int |E(\lambda)|^6 dV/V$, which characterize the 2PA and 3PA of the Si nanoparticle (see the Supplemental Material, S4 [24]). Therefore, the spectra of 2PA and 3PA can be employed to examine the blue shift of the MD resonance.

Physically, the spectra of 2PA and 3PA can be obtained by measuring the excitation spectra of the hot-electron luminescence, as shown in Fig. 2. At a low excitation intensity of 0.65 mJ/cm^2, the absorption peak coincides with the MD resonance in the scattering spectrum. When the excitation intensity is increased to 1.05 mJ/cm^2, however, the absorption peak is blue shifted by approximately 30 nm. This indicates that the maximum blue shift of the MD resonance can be observed in the steady characterization of the multiphoton-induced absorption, although it is a dynamical process. We also measure the luminescence decay of the Si nanosphere. A lifetime of approximately 30 ps is derived (see the Supplemental Material, S4), which is short enough for virtualization of the dynamical shift of the MD resonance.

From the decomposed scattering spectra of a Si nanoparticle, it is found that the MQ resonance possesses the largest quality factor, implying the largest enhancement in both the absorption and the emission (see the Supplemental Material, S5 [24]). Therefore, it can be utilized to create dense electron-hole plasmas. In the experiments, we vary the excitation wavelength around the MQ resonance and record the luminescence spectra around the MD resonance, as shown in Fig. 3. A blue shift of the luminescence peak as large as approximately 35 nm is observed when the MQ resonance is resonantly excited. In Fig. 3(b), we present the dependencies of the luminescence peak and intensity on the excitation wavelength. As expected, the strongest luminescence intensity and largest blue shift are obtained at the MQ resonance.

Similar to the MQ resonance, the resonant excitation of the EQ resonance, where the absorption of Si is larger, can also be exploited to generate a large carrier density. For another Si nanosphere, we first fix the excitation wavelength at the EQ resonance (approximately 532 nm) and raise the excitation intensity. A blue shift of the luminescence peak up to approximately 50 nm is observed, as shown in Fig. 4(a). In the inset, we present the simulated evolution of the luminescence spectrum with increasing carrier density, assuming that the radiative recombination rate is a constant and the luminescence intensity is proportional to the carrier density. A reduction in the luminescence intensity is expected when the carrier density exceeds a critical value. The physical origin is the rapid decrease of the enhancement factor with increasing carrier density [see Fig. 1(c)]. Surprisingly, such a reduction is not observed, as shown in Fig. 4(a). Instead, it is interesting to note that the luminescence intensity increases rapidly at high carrier densities.

Physically, the carrier density generated in a Si nanoparticle can be extracted from the blue shift of the luminescence peak. However, the red shift of the MD resonance induced by the temperature rise, which counteracts the blue shift described above, needs to be taken into account. Basically, an increase in the temperature leads to a reduction in
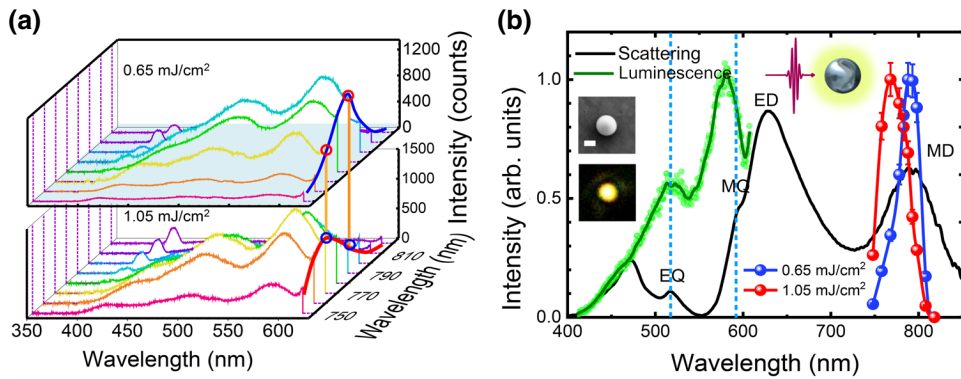
FIG. 2. The MD resonance shift revealed in the excitation spectrum of hot-electron luminescence. (a) Luminescence spectra measured for a Si nanosphere with $d \sim 200$ nm at different excitation wavelengths with two excitation intensities of 0.65 and 1.05 mJ/cm^2. (b) Excitation spectra measured at two excitation intensities of 0.65 and 1.05 mJ/cm^2. The scattering and hot-electron luminescence spectra for the Si nanosphere are also provided for reference. The scanning-electron-microscope image of the Si nanosphere and the image of the hot-electron luminescence recorded using a charge-coupled device are shown in the insets.

the band-gap energy, which in turn results in an increase in the refractive index [22], as shown in Fig. 4(b). Therefore, the carrier density resulting from the blue shift of the luminescence peak is underestimated. Theoretically, we can calculate the dependence of the temperature of a Si nanoparticle on the number of irradiated femtosecond laser pulses [32–34], as shown in the inset (see the Supplemental Material, S6 [24]). It can be seen that the steady temperature in the Si nanoparticle exhibits a dependence on the excitation intensity. Based on this relationship, one can more accurately derive the carrier density generated in the Si nanoparticle.

As mentioned above, an intriguing phenomenon observed in the experiments is the rapid increase of the luminescence intensity at high carrier densities, as shown in Fig. 4(a). In order to gain a deep insight into this behavior, we examine the enhancement factor spectra for different excitation intensities by using the luminescence spectrum obtained at a low excitation intensity of 0.85 mJ/cm^2 as a reference, as shown in Fig. 4(c). At low excitation intensities, the enhancement factor is almost

independent of the emission wavelength. At a high excitation intensity of 2.89 mJ/cm^2, larger enhancement factors are observed at approximately 850 nm and approximately 650 nm, where the MD and ED resonances are located, implying a more rapid increase in the luminescence intensity. It is also remarkable that the enhancement factor increases rapidly, from approximately 10 to approximately 26, at the MD and ED resonances when the excitation intensity is raised slightly from 2.38 to 2.89 mJ/cm^2, implying a rapid increase in the radiative recombination rate. Physically, the radiative recombination rate becomes proportional to the carrier density in the case of large injection [35], leading to the rapid increase in the luminescence intensity. This behavior means that amplification of spontaneous emission may be realized by creating dense electron-hole plasmas in a Si nanoparticle.

Given knowledge of the carrier density generated in a Si nanoparticle, the quantum efficiency of the Si nanoparticle ($\eta = N_{photon}/N_{eh}$) can be deduced because the emitted photons can be readily estimated from the integration of
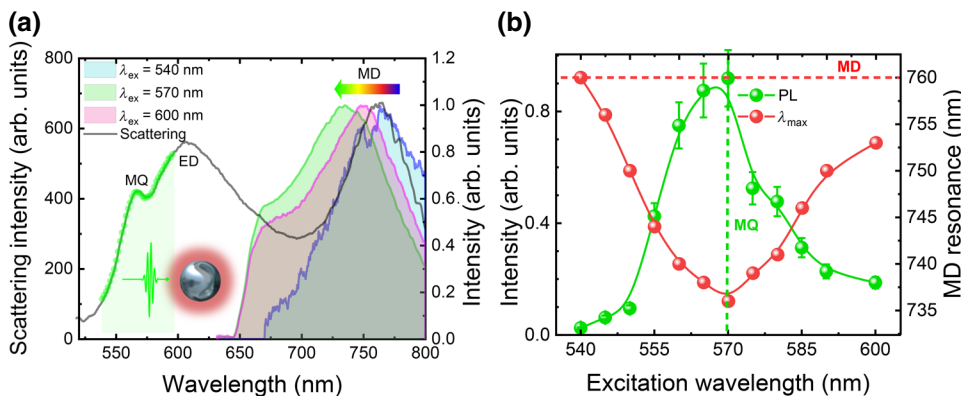

FIG. 3. The MD resonance shift revealed in the MD-enhanced hot luminescence. (a) Hot-electron luminescence spectra measured for a Si nanosphere excited at different wavelengths of 540, 570, and 600 nm. The scattering spectrum measured for the Si nanosphere is also provided for reference. (b) The dependence of the PL intensity and MD resonance on the excitation wavelength.
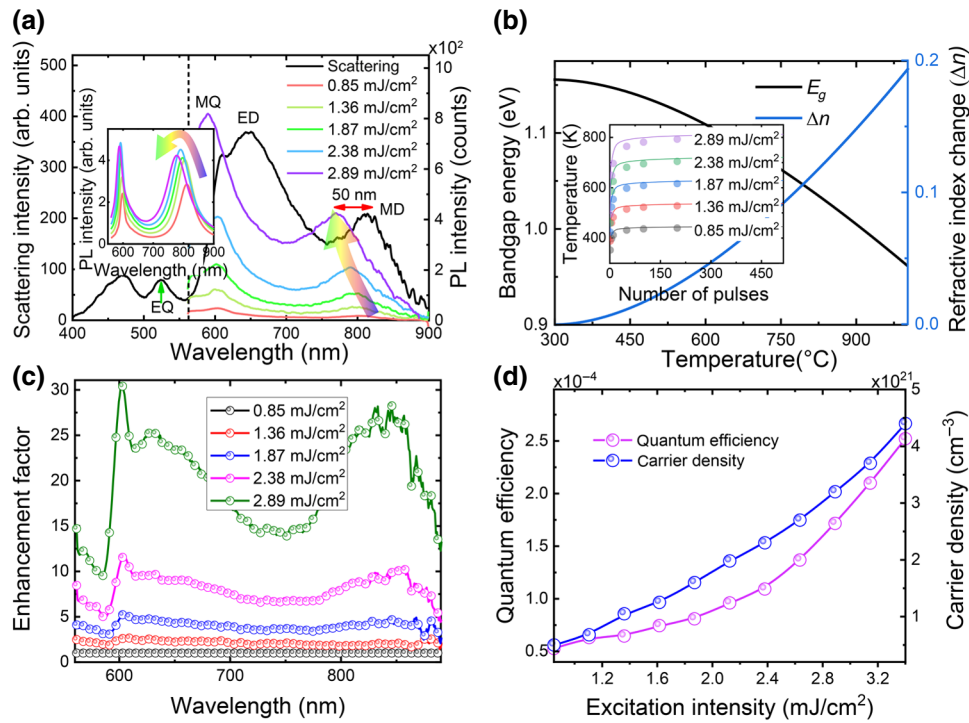
FIG. 4. The enhanced quantum efficiency observed at high carrier densities. (a) Hot-electron luminescence spectra measured for a Si nanosphere, which is excited at 530 nm, at different excitation intensities. The evolution of the luminescence spectrum with increasing carrier density simulated for the Si nanosphere is shown in the inset. (b) The dependence of the band-gap energy and the refractive-index change of Si on the temperature. The dependence of the temperature on the number of irradiated pulses calculated for a Si nanosphere with $d \sim 200$ nm is shown in the inset. (c) The wavelength dependence of the enhancement factor for the hot-electron luminescence calculated at different excitation intensities. (d) The dependence of the quantum efficiency and carrier density on the excitation intensity extracted for the Si nanosphere.

the luminescence spectrum of the Si nanoparticle characterized by the photon counts [14]. In Fig. 4(d), we present the dependence of the quantum efficiency on the excitation intensity derived for the Si nanoparticle. Interestingly, a rapid increase in the quantum efficiency is observed at high excitation intensities owing to the increase in the radiative recombination rate. Therefore, the enhanced radiative recombination rate induced by dense electron-hole plasmas may counteract or even surpass the reduction of the enhancement factor, leading to the appearance of amplified spontaneous emission in Si nanoparticles. Similar behavior has been observed if we choose to resonantly excite the MQ resonance of a Si nanosphere (see the Supplemental Material, S7 [24]).

Previously, bistability and self-modulation phenomena have been commonly observed in Si microresonators, including microrings, microdisks, and photonic crystal cavities, owing to the cooperation of various nonlinear optical effects and the temperature effect [36–38]. It is noted, however, that these cavities possess very large Q factors (approximately 10^5) and that a continuous-wave laser light with a very narrow line width is generally employed as the excitation source. When the excitation

intensity exceeds a threshold, the competing resonance shifts (i.e., the red shift induced by the thermo-optic effect and the blue shift induced by the free carrier dispersion) result in a modulation of the resonance wavelength temporally and periodically. In comparison, the Q factors of the Mie resonances in a Si nanopartcle, ranging from 5 to 50, are several orders of magnitude lower than those of Si microresonators. In addition, the excitation source in our case is femtosecond laser pulses with a wide line width of approximately 10 nm. For carrier injection, we can choose either resonant or nonresonant excitation of the MQ and/or EQ resonances. In the latter case, no bistability and self-modulation phenomena are expected because only the emission at the MD resonance is examined. Even in the case of resonant excitation, we do not observe any bistability and self-modulation behavior because of the absence of any feedback mechanism. As can be seen in Fig. 4(b), the temperature rise induced in a Si nanoparticle, which depends on the laser fluence, reaches a constant value after irradiating approximately 100 laser pulses. As a result, the refractive-index change of Si and the induced wavelength shifts in the Mie resonances also become steady values for a fixed laser fluence. In sharp contrast, the refractive-index

change of Si induced by injected free carriers only occurs for the duration of the excitation laser pulses (approximately 130 fs) and it disappears about 30 ps after the laser pulses through radiative recombination, giving rise to the hot-electron luminescence observed in the experiments. Therefore, the blue shift of the MD resonance observed in the hot-electron luminescence is the maximum blue shift recorded by the transient luminescence subtract the steady red shift induced by the temperature rise.

IV. CONCLUDING REMARKS

In summary, we propose a strategy to characterize the blue shift of the MD resonance of a Si nanoparticle induced by dense electron-hole plasmas by exploiting the MD-enhanced luminescence emitted by the Si nanoparticle. It is found that the MD resonance of the Si nanoparticle is blue shifted, broadened, and attenuated with increasing carrier density. The maximum blue shift of the MD resonance can be characterized by the steady blue shift of the multiphoton-induced absorption peak or the hot-electron luminescence peak, from which the carrier density and quantum efficiency of the Si nanoparticle can be derived. The luminescence intensity or the quantum efficiency exhibits a rapid increase at high carrier densities, implying an increase in the radiative recombination rate. Here, we demonstrate that the quantum efficiency of the hot-electron luminescence of silicon nanoparticles can be enhanced by a factor of more than 5 through injecting dense electron-hole plasmas. Our findings indicate the possibilities for manipulating the hot-electron luminescence from Si nanoparticles [39] and for realizing amplified spontaneous emission, which will contribute to the making of efficient Si-based light-emitting devices for integrated photonic circuits in the future.

ACKNOWLEDGMENTS

[1] F. Priolo, T. Gregorkiewicz, G. Matteo, and F. Krauss, Silicon nanostructures for photonics and photovoltaics, Nat. Nanotechnol. **9**, 19 (2014).

[2] W. D. A. M. de Boer, D. Timmerman, K. Dohnalova, I. N. Yassievich, H. Zhang, W. J. Buma, and T. Gregorkiewicz, Red spectral shift and enhanced quantum efficiency in phonon-free photoluminescence from silicon nanocrystals, Nat. Nanotechnol. **5**, 878 (2010).

[3] N. Yu and F. Capasso, Flat optics with designer metasurfaces, Nat. Mater. **13**, 139 (2014).

[4] N. Meinzer, W. L. Barnes, and I. R. Hooper, Plasmonic meta-atoms and metasurfaces, Nat. Photonics **8**, 889 (2014).

[5] M. Khorasaninejad, W. T. Chen, R. C. Devlin, J. Oh, A. Y. Zhu, and F. Capasso, Metalenses at visible wavelengths: Diffraction-limited focusing and subwavelength resolution imaging, Science **352**, 1190 (2016).

[6] J. B. Pendry, A. J. Holden, W. J. Stewart, and I. Youngs, Extremely Low Frequency Plasmons in Metallic Mesostructures, Phys. Rev. Lett. **76**, 4773 (1996).

[7] J. B. Pendry, A. J. Holden, D. J. Robbins, and W. J. Stewart, Magnetism from conductors and enhanced nonlinear phenomena, IEEE Trans. Microwave Theory Tech. **47**, 2075 (1999).

[8] I. Staude and J. Schilling, Metamaterial-inspired silicon nanophotonics, Nat. Photonics **11**, 274 (2017).

[9] A. I. Kuznetsov, A. E. Miroshnichenko, M. L. Brongersma, Y. S. Kivshar, and Boris Luk'yanchuk, Optically resonant dielectric nanostructures, Science **354**, aag2472 (2016).

[10] J. C. Ginn, I. Brener, D. W. Peters, J. R. Wendt, J. O. Stevens, P. F. Hines, L. I. Basilio, L. K. Warne, J. F. Ihlefeld, P. G. Clem, and M. B. Sinclair, Realizing Optical Magnetism from Dielectric Metamaterials, Phys. Rev. Lett. **108**, 097402 (2012).

[11] Y. H. Fu, A. I. Kuznetsov, A. E. Miroshnichenko, Y. F. Yu, and B. Luk'yanchuk, Directional visible light scattering by silicon nanoparticles, Nat. Commun. **4**, 1527 (2013).

[12] M. F. Picardi, A. V. Zayats, and F. J. Rodriguez-Fortuno, Janus and Huygens Dipoles: Near-Field Directionality beyond Spin-Momentum Locking, Phys. Rev. Lett. **120**, 117402 (2018).

[13] J. Xiang, S. Jiang, J. D. Chen, J. Li, Q. Dai, C. Zhang, Y. Xu, S. Tie, and S. Lan, Hot-electron intraband luminescence from GaAs nanospheres mediated by magnetic dipole resonances, Nano Lett. **17**, 4853 (2017).

[14] C. Zhang, Y Xu, J. Liu, J. Li, J. Xiang, H. Li, J. Li, Q. Dai, S. Lan, and A. E. Miroshnichenko, Lighting up silicon nanoparticles with Mie resonances, Nat. Commun. **9**, 2964 (2018).

[15] A. F. Cihan, A. G. Curto, S. Raza, P. G. Kik, and M. L. Brongersma, Silicon Mie resonators for highly directional light emission from monolayer MoS_2, Nat. Photonics **12**, 284 (2018).

[16] A. L. Holsteen, S. Raza, P. Fan, P. G. Kik, and M. L. Brongersma, Purcell effect for active tuning of light scattering from semiconductor optical antennas, Science **358**, 1407 (2017).

[17] J. Yang, C. Ma, P. Liu, C. Wang, and G. Yang, Electrically controlled scattering in a hybrid dielectric-plasmonic nanoantenna, Nano Lett. **17**, 4793 (2017).

[18] M. R. Shcherbakov, S. Liu, V. V. Zubyuk, A. Vaskin, P. P. Vabishchevich, G. Keeler, T. Pertsch, T. V. Dolgova, I. Staude, I. Brener, and A. A. Fedyanin, Ultrafast all-optical

tuning of direct-gap semiconductor metasurfaces, Nat. Commun. **8,** 17 (2017).

[19] A. Rudenko, K. Ladutenko, S. Makarov, and T. E. Itina, Photogenerated free carrier-induced symmetry breaking in spherical silicon nanoparticle, Adv. Opt. Mater. **6,** 1701153 (2018).

[20] S. Makarov, S. Kudryashov, I. Mukhin, A. Mozharov, V. Milichko, A. Krasnok, and P. Belov, Tuning of magnetic optical response in a dielectric nanoparticle by ultrafast photoexcitation of dense electron-hole plasma, Nano Lett. **15,** 6187 (2015).

[21] D. G. Baranov, S. V. Makarov, A. E. Krasnok, P. A. Belov, and A. Alu, Tuning of near- and far-field properties of all-dielectric dimer nanoantennas via ultrafast electron-hole plasma photoexcitation, Laser Photonics Rev. **10,** 1009 (2016).

[22] M. Rahmani, L. Xu, A. E. Miroshnichenko, A. Komar, R. Camacho-Morales, H. Chen, Y. Zrate, S. Kruk, G. Zhang, D. N. Neshev, and Y. S. Kivshar, Reversible thermal tuning of all-dielectric metasurfaces, Adv. Funct. Mater. **27,** 1700580 (2017).

[23] K. Sokolowski-Tinten and D. von der Linde, Generation of dense electron-hole plasmas in silicon, Phys. Rev. B **61,** 2643 (2000).

[24] See the Supplemental Material at http://link.aps.org/supplemental/10.1103/PhysRevApplied.13.014003 for the SEM and TEM characterization of the Si nanoparticles, the dependence of the dielectric constant of Si on the carrier density, the internal mode volume calculated for the Si nanospheres, the electric field enhancement factors calculated at the Mie resonances, the luminescence decay measured for the Si nanoparticles, the temperature rise in the Si nanoparticles induced by femtosecond laser pulses, and the optical responses of the Si nanoparticles resonantly excited at their EQ resonances.

[25] LUMERICAL, commercial software developed by Lumerical Solutions Inc. (http://www.lumerical.com).

[26] J. Xiang, J. Li, Z. Zhou, S. Jiang, J. Chen, Q. Dai, S. Tie, S. Lan, and X. Wang, Manipulating the orientations of the electric and magnetic dipoles induced in silicon nanoparticles for multicolor display, Laser Photonics Rev. **12,** 1800032 (2018).

[27] T. Ming, H. Chen, R. Jiang, Q. Li, and J. Wang, Plasmon-controlled fluorescence: Beyond the intensity enhancement, J. Phys. Chem. Lett. **3,** 191 (2012).

[28] J. Mertens, M.-E. Kleemann, R. Chikkaraddy, P. Narang, and J. J. Baumberg, How light is emitted by plasmonic metals, Nano Lett. **17,** 2568 (2017).

[29] Y. Fang, W. Chang, B. Willingham, P. Swanglap, S. Dominguez-Medina, and S. Link, Plasmon emission quantum yield of single gold nanorods as a function of aspect ratio, ACS Nano **6,** 7177 (2012).

[30] L. D. Landau, J. Bell, M. Kearsley, L. Pitaevskii, E. Lifshitz, and J. Sykes, *Electrodynamics of Continuous Media* (Elsevier Butterworth-Heinemann, Oxford, 1984), Vol. 8.

[31] A. B. Evlyukhin, T. Fischer, C. Reinhardt, and B. N. Chichkov, Optical theorem and multipole scattering of light by arbitrarily shaped nanoparticles, Phys. Rev. B **94,** 2469 (2016).

[32] P. Zijlstra, J. W. M. Chon, and M. Gu, Effect of heat accumulation on the dynamic range of a gold nanorod doped polymer nanocomposite for optical laser writing and patterning, Opt. Express **15,** 12151 (2007).

[33] Q. Dai, M. Ouyang, W. Yuan, J. Li, B. Guo, S. Lan, S. Liu, Q. Zhang, G. Lu, S. Tie, H. Deng, Y. Xu, and M. Gu, Encoding random hot spots of a volume gold nanorod assembly for ultralow energy memory, Adv. Mater. **29,** 1701918 (2017).

[34] G. P. Zograf, M. I. Petrov, D. A. Zuev, P. A. Dmitriev, V. A. Milichko, S. V. Makarov, and P. A. Belov, Resonant non-plasmonic nanoparticles for efficient temperature feedback optical heating, Nano Lett. **17,** 2945 (2017).

[35] Sheng S. Li, *Semiconductor Physical Electronics* (Springer-Verlag, Berlin/Heidelberg/New York, 2006), Chap. 6.

[36] T. J. Johnson, M. Borselli, and O. Painter, Self-induced optical modulation of the transmission through a high-Q silicon microdisk resonator, Opt. Express **14,** 817 (2006).

[37] J. Yang, T. Gu, J. Zheng, M. Yu, G. Q. Lo, D. L. Kwong, and C. Wei Wong, Radio frequency regenerative oscillations in monolithic high-Q/V heterostructured photonic crystal cavities, Appl. Phys. Lett. **104,** 061104 (2014).

[38] S. Chen, L. Zhang, Y. Fei, and T. Cao, Bistability and self-pulsation phenomena in silicon microring resonators based on nonlinear optical effects, Opt. Express **20,** 7454 (2012).

[39] S. V. Makarov, A. S. Zalogina, M. Tajik, D. A. Zuev, M. V. Rybin, A. A. Kuchmizhak, S. Juodkazis, and Y. Kivshar, Light-induced tuning and reconfiguration of nanophotonic structures, Laser Photonics Rev. **11,** 1700108 (2017).